

NSG 22-009015

## The Response Function of Modulated Grid Faraday Cup Plasma Instruments

by Alan Barnett and Stanislaw Olbert

Massachusetts Institute of Technology, Cambridge, Massachusetts

MS 700 802

IN-9134

## Abstract

Modulated grid Faraday cup plasma analyzers are a very useful tool for making in situ measurements of space plasmas. One of their great attributes is that their simplicity permits their angular response function to be calculated theoretically. In this paper, we derive an expression for this response function by computing the trajectories of the charged particles inside the cup. We use the Voyager Plasma Science (PLS) experiment as a specific example. Two approximations to the "rigorous" response function useful for data analysis are discussed.

The theoretical formulas were tested by multi-sensor analysis of solar wind data. The tests indicate that the formulas represent the true cup response function for all angles of incidence with a maximum error of only a few percent.

Rev. of Sci. Instrum.

(NASA-CR-177312) THE RESPONSE FUNCTION OF  
MODULATED GRID FARADAY CUP PLASMA  
INSTRUMENTS (Massachusetts Inst. of Tech.)  
37 p HC A03/MF A01

N86-27076

CSCL 201

G3/75 Unclas  
43475

## 1. Introduction

Since the earliest days of space exploration, space probes have included instruments to measure plasma particles. There are two broad classes of plasma instruments; the modulated grid Faraday cup and the electrostatic analyzer. Modulated grid Faraday cups consist of a collector and several grids. The operation of such detectors is the topic of the bulk of this paper. Electrostatic analyzers typically consist of two curved conducting plates, with a potential difference between them and a particle counter at one end. When particles enter the instrument, only those particles moving in the proper direction with the proper energy-per-charge reach the collector. A good review article on techniques of deep-space plasma measurements is by Vasyliunas<sup>1</sup>.

The first successful American spacecraft to carry a plasma probe was Explorer 10, launched in 1961. This instrument, which was the first to provide direct evidence of the existence of the solar wind<sup>2</sup> (it actually measured the flow in the magnetosheath), was a modulated grid Faraday cup. The existence of the solar wind was confirmed and became generally accepted after observations made by Mariner 2, which carried an electrostatic analyzer<sup>3</sup>.

As more missions were flown, the plasma instruments improved. In order to measure the solar wind direction, Faraday cups with segmented collector plates were flown. If the plasma flow direction differs from normal to the cup, the current to the individual segments differs due to the shadow of the aperture. Faraday cups with three segments were flown on Mariner 4 and 5, which were 3-axis stabilized spacecraft<sup>4, 5</sup>, while a cup with its collector divided into two segments was flown on each of the spin-stabilized spacecraft Pioneer 6 and 7<sup>6, 7</sup> and Explorer 33<sup>8</sup>.

Improved sensitivity to the flow angle can be obtained by using an array of Faraday cups, each of which is pointed in a different direction. An instrument consisting of an array of four Faraday cups which was flown on the Voyager missions to the outer planets<sup>9</sup> is shown in Figure 1. This instrument has successfully measured positive ions and electrons in the solar wind<sup>10</sup>, and at Jupiter<sup>11, 12</sup> and Saturn<sup>13</sup>. For the case of a cold beam of particles (such as the solar wind) flowing in a direction close to the look direction of the cups, data analysis from these instruments is straightforward. For cases when either the flow direction is not close to the look direction of the cups, or the plasma thermal speed is comparable to or greater than the bulk velocity, or both, detailed knowledge of the instrument response function is required for the data analysis. The full response function described below has already been used for the study of the plasma flow around the Io flux tube<sup>14</sup>, and further work utilizing it is in progress.

In this paper we discuss the operation of this type of instrument and derive an expression for its response function. Although the formulas which we quote describe the Voyager instrument, the method we use can easily be applied to any Faraday cup.

The response function of the cup is defined as the ratio of the particle flux reaching the collector to the particle flux incident on the aperture when the incident particles are a collimated, monoenergetic beam. We compute the response function by studying the trajectories of the particles inside the cup. In Section 2 we describe the model of the cup which we use and the nature of the approximations which we have to make.

We show that the response function can be written as a product of two terms, the "sensitive area" and the grid transparency. The sensitive area

term is computed from a straightforward study of the trajectories, while statistical arguments are required to determine the grid transparency term. These terms are derived in detail, and explicit expressions for them are given for the case of the Voyager instruments, in Sections 3 and 4.

Once the response function is known, one can use it to analyze data. The collector current from a plasma described by a known distribution function can be computed by performing an integration over velocity space. The problem of data analysis, therefore, becomes the problem of solving an integral equation for the distribution function. A very useful approximate method for solving the integral equation is to use a parameterized model for the distribution function, and then find the "best fit" values for the parameters. In order to do this, one must be able to perform the velocity space integration. Certain further approximations which permit the integration over the components of velocity perpendicular to the cup normal to be performed analytically for the case where the distribution function is a convected maxwellian are described in Section 5.

Once we have computed the response function, we want to test it. In order to do this, one would like to have a very narrow test beam. Unfortunately, it is very difficult to make such a beam in the lab. We have used the calm solar wind at about 4 AU as our test beam. Analysis of data from Voyager 1 taken when the spacecraft was rotating (Voyager is a three axis stablized spacecraft) causing the solar wind to enter the cups at large angles indicates that our expressions are an excellent representation of the true response functions of the cups for all energies and angles of incidence. This analysis is discussed in Section 6.

## 2. The Physics of the Modulator Grid Faraday Cup

In this section, we analyze the physics of the Faraday cup and present the model which we use to compute the response function, using the Voyager Plasma Science (PLS) instrument as an example. Throughout this paper, we will consider the measurement of positive ions. For electrons, the analysis which we present can be modified in a straightforward manner, although in that case the emission of secondaries must be considered.

As can be seen from Figure 1, the PLS instrument consists of 4 Faraday cups. Three of them, called the A, B, and C cups are arrayed about an axis of symmetry and have pentagonally shaped apertures and collectors. The fourth cup, called the D-cup, is circular in shape (a more conventional design) and points  $88^\circ$  from the main sensor symmetry axis. The geometry will be very important for understanding the test of the response function.

A cross-section of one of the PLS instrument's main sensor cups is shown in Figure 2. The cup consists of an aperture stop, eight parallel grids and a collector plate mounted in a metal housing. A top view of a cup is shown in Figure 3. Fig. 3 also defines a coordinate system which we call cup coordinates ( $\hat{z}$  is the inward pointing cup normal). Notice that the collector is much larger than the aperture, a fact which gives this cup a much larger field of view than a conventional cup.

During operation, the collector plate and all of the grids except the modulator grids and the suppressor grid are grounded to the spacecraft. The suppressor grid is kept at -95 V to shield the collector from the plasma electrons and to return any secondary electrons to the collector. The instrument is used by applying a square wave positive voltage to the modulator grids and measuring the collector current. Since more particles are repelled

when the retarding potential is increased, the current waveform is an inverted square wave as shown in Figure 4. We call the upper and lower limiting modulator voltages  $\phi_k$  and  $\phi_{k+1}$ , respectively, and the corresponding collector currents  $I_k^*$  and  $I_{k+1}^*$ . The signal  $I_k$  is the amplitude of the current step, given by

$$I_k = I_k^* - I_{k+1}^* \quad 1$$

We wish to determine collector current as a function of the modulator voltage and the plasma distribution function. To a first approximation, the signal consists of all of the incident particles for which the z-component of velocity ( $v_z$ ) is between  $v_k$  and  $v_{k+1}$ , where  $v_k$  is related to  $\phi_k$  by

$$v_k = (2Z^* e \phi_k / A^* m_p)^{1/2} \quad 2$$

where  $m_p$  is the proton mass,  $A^*$  is the mass of the ion in AMU,  $Z^*$  is the charge state of the ion, and  $e$  is the proton charge. To obtain a better approximation, we need to study the motion of the charged particles inside the cup.

The total electric current incident on the aperture ( $I_{ap}$ ) due to ionic species  $a$  is

$$I_{ap} = Z_a^* e \iint_{\text{Aperture}} dx dy \int_{-\infty}^{\infty} dv_x \int_{-\infty}^{\infty} dv_y \int_0^{\infty} v_z f_a(\vec{v}) dv_z \quad 3$$

where  $dx dy$  is an area element in the aperture and  $f_a(\vec{v})$  is the distribution function of ion species  $a$ . For the total current, one must sum over all species. In the remainder of this paper, we will suppress the subscript  $a$ .

Not all of the particles incident on the aperture reach the collector. In principle, given the initial position and velocity of a particle, one can calculate its trajectory and thereby determine whether or not it will reach

the collector. We can therefore formally write for the collector current

$$I_k^* = Z^* e \iint_{\text{Aperture}} dx dy \int_{-\infty}^{\infty} dv_x \int_{-\infty}^{\infty} dv_y \int_0^{\infty} v_z f(\vec{v}) H(\vec{v}, x, y, \phi_k) dv_z \quad 4$$

where  $H(\vec{v}, x, y, \phi_k)$  is equal to one if the trajectory of a particle incident on the aperture at the position  $x, y$  with velocity  $\vec{v}$  reaches the collector, and is equal to zero otherwise. In practice, Equation 4 is useless in this form because the precision with which we can calculate the particle trajectories is insufficient to permit us to accurately predict whether or not a given incident particle will collide with one of the grids. We can, however, compute the probability that a particle will collide with a grid. If we denote by  $A_{ap}$  the area of the aperture, and by  $R(\vec{v}, \phi_k)$  the probability that an incident particle with velocity  $\vec{v}$  has of reaching the collector (which is the same as the fraction of particles of a uniform beam of particles with velocity  $\vec{v}$  which reaches the collector), we can rewrite the Equation 4 as

$$I_k^* = Z^* e A_{ap} \int_{-\infty}^{\infty} dv_x \int_{-\infty}^{\infty} dv_y \int_0^{\infty} v_z f(\vec{v}) R(\vec{v}, \phi_k) dv_z \quad 5$$

We call  $R(\vec{v}, \phi_k)$  the response function of the detector.

To determine  $R$ , we use the following model of the cup. We assume that the electrostatic potential inside the cup depends only on  $z$ , and that it is a linear function of distance between any two adjacent grids. (The model potential for the Voyager PLS main sensor cups is shown in Figure 5.) This approximation neglects the fine structure of the fields near the grid wires and the fringing fields near the edges of the grids. Since the distance between the grids is much greater than the spacing between the wires and the grid spacing is much smaller than the linear dimensions of the grid, this approximation should be adequate.

In our model field, we can calculate the particle trajectories exactly. The particle trajectory between any two grids is either a straight line or a parabola. If we now assume that the probability of a particle striking a grid (a possibility not included in our trajectory calculation) does not depend on the position where the particle enters the cup, we can write  $R$  as a product of two terms and a normalization constant

$$R(\vec{v}, \phi_k) = T(\vec{v}, \phi_k) A(\vec{v}, \phi_k) / A_{ap} \quad 6$$

where  $T$  is the transparency of the grids (the probability that a particle does not collide with a grid),  $A$  is the "sensitive area" (the area of the aperture for which incident particles will strike the collector).

### 3. The Sensitive Area

We discuss first the sensitive area. Consider an incident beam of particles of velocity  $\vec{v}$ . If  $v_z$  is less than  $v_k$ , defined by Equation 2, then the particle will be repelled by the modulator voltage, so  $R$  will be 0. We take this into account by changing, in Equation 5, the lower limit of integration over  $v_z$  from zero to  $v_k$ .

If  $v_z$  is greater than  $v_k$ , then in the collector plane the beam will have the shape of the aperture, but its position will be displaced because of the components of the particle velocity transverse to the cup normal direction, as shown in Figure 6. We define a two-dimensional vector  $\vec{S}$ , also shown in Figure 6, to be the displacement of the aperture image from a perpendicular projection of the aperture into the plane of the collector. One can calculate



from the equations of motion that the "shift vector"  $\vec{S}$  is given by

$$S_x = S^* h \frac{v_x}{v_z} \quad 7a$$

$$S_y = S^* h \frac{v_y}{v_z} \quad 7b$$

where  $h$  is the distance between the aperture and the collector, and  $S^*$ , called the shift function, depends only upon  $v_z$ , the cup geometry, and the grid voltages. For the Voyager main sensor cups, the shift function is given explicitly by

$$S^* = .743 \left( \frac{[1 - (1 - \frac{v_k^2}{v_z^2})^{1/2}]}{(v_k^2/v_z^2)} \right) + .093 \left( \frac{1}{1 - (v_k^2/v_z^2)} \right)^{1/2} + .392 \left( \frac{[(1 + \frac{v_s^2}{v_z^2})^{1/2} - 1]}{(v_s^2/v_z^2)} \right) + .340 \quad 8$$

The subscript  $s$  refers to the suppressor grid;  $v_s$  is defined in a manner analogous to the definition of  $v_k$  in Equation 2

$$v_s = |2Z^* e \phi_s / A^* m_p|^{1/2} \quad 9$$

where  $\phi_s$  is the voltage on the suppressor grid.

Once the shift vector is known, the sensitive area can be computed in a straightforward manner using a geometrical construction. For cups with cylindrical symmetry, the sensitive area depends only on the magnitude of  $\vec{S}$ , and the functional dependence can be expressed simply in closed form. For the Voyager main sensor, on the other hand, this functional dependence is complicated. As there are 16 separate regions where the dependence is different (see Figure 7), an exact analytical representation is cumbersome. A plot of the sensitive area (normalized to unity for normal incidence) as a function of  $S_y/h$ , with  $S_x/h$  as a parameter, is shown in Figure 8.

#### 4. The Grid Transparency

We now consider the grid transparency. The transparency of a single grid is defined as the probability of an incident particle traversing the plane of the grid without colliding with the wires (all particles which strike the wires are assumed to be absorbed). We model a grid as a planar structure consisting of two perpendicular sets of parallel cylindrical wires. The transparency of the grid will be the product of the transparencies of each set of wires considered separately.

Consider a set of wires which run in the  $\hat{y}$ -direction (as before,  $\hat{z}$  is taken to be normal to the plane of the grid). Since the transparency of these wires does not depend upon  $v_y$ , we only need to consider the projection of the particle motion into the  $x$ - $z$  plane. The probability of a particle colliding with one of the wires is simply the ratio of the area of the wires to the area of the gaps between the wires projected into a plane perpendicular to the particle velocity vector. As can be seen from Figure 9, the probability of collision is proportional to  $\sec \alpha$ , where  $\alpha$  is the angle between the projection of the particle velocity into the  $x$ - $z$  plane and the  $z$ -axis. The same line of reasoning can be applied to the set of wires which runs in the  $\hat{x}$ -direction. Using the computed trajectories in our simplified cup model to compute the value of  $\alpha$  for each grid, and noting that the probability of a particle reaching the collector plane without colliding with a grid is simply the product of the probabilities of it successfully traversing each individual grid, we can write the grid transparency term as the following product

$$T = \prod_{i=1}^N \left[ 1 - c \left( 1 + \frac{v_x^2}{v_z^2 - \frac{2Z^* e \phi_i}{A^* m_p}} \right)^{1/2} \right] \left[ 1 - c \left( 1 + \frac{v_y^2}{v_z^2 - \frac{2Z^* e \phi_i}{A^* m_p}} \right)^{1/2} \right] \quad 10$$

where  $\phi_i$  is the voltage on the  $i$ -th grid,  $c$  is the ratio of the wire diameter to the wire spacing, and  $N$  is the total number of grids.

For the voyager main sensor,  $c=1/42$  and the sets of wires in the different grids are parallel. Since each cup has three modulator grids, one suppressor grid, and five grounded grids (see Fig. 1), the transparency is given explicitly by

$$T = [1 - c(1 + \frac{v_x^2}{v_z^2})^{1/2}]^5 [1 - c(1 + \frac{v_x^2}{v_z^2 - v_k^2})^{1/2}]^3 [1 - c(1 + \frac{v_x^2}{v_z^2 + v_s^2})^{1/2}] \times$$

$$[1 - c(1 + \frac{v_y^2}{v_z^2})^{1/2}]^5 [1 - c(1 + \frac{v_y^2}{v_z^2 - v_k^2})^{1/2}]^3 [1 - c(1 + \frac{v_y^2}{v_z^2 + v_s^2})^{1/2}]$$

11

For the Voyager main sensor cups at normal incidence,  $T=T_0=(1-c)^{18}=0.65$ .

## 5. Further Approximations

In order to use our results to analyze data, one must evaluate the integrals of Equation 5 for a parameterized distribution function, and use the data to obtain "best fit" values for the parameters. It is possible to do all of the integrations numerically, but a much faster running computer code can be written if some of the integrations can be done analytically. In this section we outline two approximation schemes which permit analytical, closed form evaluation of the integrations over  $v_x$  and  $v_y$ . The details of the schemes are given in reference 15.

For the complicated geometry of the Voyager PLS main sensor, a suitable analytic expression for the sensitive area (Figure 8) must first be found. We used a family of trapezoids, plotted in Figure 10. The formulas for these trapezoids are

$$A = A_x(S_x/h)A_y(S_x/h, S_y/h) \quad 12$$

$$A_x = \frac{(S_x/h) + X'_r}{X'_r - X_r} \quad -X'_r < S_x/h < -X_r \quad 12a$$

$$A_x = 1 \quad -X_r < S_x/h < X_r \quad 12b$$

$$A_x = -\frac{(S_x/h) - X'_r}{X'_r - X_r} \quad X_r < S_x/h < X'_r \quad 12c$$

$$A_x = 0 \quad \text{Otherwise} \quad 12d$$

$$A_y = \frac{(S_y/h) - Y'_d}{Y_d - Y'_d} \quad Y'_d < S_y/h < Y_d \quad 12e$$

$$A_y = 1 \quad Y_d < S_y/h < Y_u(S_x) \quad 12f$$

$$A_y = \frac{(S_y/h) - Y'_u(S_x)}{Y_u(S_x) - Y'_u(S_x)} \quad Y_u(S_x) < S_y/h < Y'_u(S_x) \quad 12g$$

$$A_y = 0 \quad \text{Otherwise} \quad 12h$$

with

$$X_r = 1.10 \quad 13a$$

$$X'_r = 4.94 \quad 13b$$

$$Y_d = -2.02 \quad 13c$$

$$Y'_d = -3.62 \quad 13d$$

$$Y_u = \frac{0.762 \cos\{1.018|S_x/h| + 0.247\}}{1 + 0.25|S_x/h|} \quad 13e$$

$$Y'_u = 2.50 - 0.125[|S_x/h| - 1]^2 \quad 13f$$

All of the quantities defined by Equations 12a-h and 13a-f are dimensionless.

$Y_u$  and  $Y'_u$  are plotted in Figure 11. Figure 12 shows a 3-D plot of  $A(\vec{S}/h)$ .

The values of  $X_r$ ,  $X'_r$ ,  $Y_d$ ,  $Y'_d$ ,  $Y_u$ , and  $Y'_u$  were chosen so as to match the volume of the solid of Fig. 12 as closely as possible with the volume of the solid representing the true area overlap. Figure 13 shows a 3-D plot of  $R(S_x/h, S_y/h)$ , computed using the "trapezoidal approximation" for A and Eq. 11 for T.

We shall now proceed to describe two different approximation schemes. In both cases, the plasma distribution function will be assumed to be a convected maxwellian

$$f(\vec{v}) = \frac{n_0}{w^3 \pi^{3/2}} \exp\{-(\vec{v}-\vec{V})^2/w^2\} \quad 14$$

where  $\vec{V}$  is the plasma bulk velocity,  $w$  is the thermal speed, and  $n_0$  is the particle number density. For the case where  $V \gg w$ , we have a well collimated beam. In this case, we can approximate the dependence of  $f$  on  $v_x$  and  $v_y$  by a product of delta functions

$$f(\vec{v}) = \frac{n_0}{w/\pi} \delta(v_x - V_x) \delta(v_y - V_y) \exp\{-(v_z - V_z)^2/w^2\} \quad 15$$

The delta functions permit the integrations over  $v_x$  and  $v_y$  to be computed trivially, leaving only the numerical integration over  $v_z$ . This approximation was used to experimentally test the response function, as described in the following section.

For the more general case where the bulk velocity is not much greater than the thermal speed, we must change the form of the expression for the grid transparency. It is possible to approximate Equation 10 by an expression of the form

$$T = \left[ \sum_{i=1}^2 c_i \exp\{-a_i \left(\frac{v_x}{v_z}\right)^2\} \right] \left[ \sum_{j=1}^2 c_j \exp\{-a_j \left(\frac{v_y}{v_z}\right)^2\} \right] \quad 16$$

where the  $a$ 's and  $c$ 's are functions of the grid voltages and  $v_z$  only. The values of the  $a$ 's and  $c$ 's must be determined by a numerical fitting procedure.

This approximation permits the desired integrals to be evaluated numerically with the aid of the saddle point method.

For a cylindrically symmetrical cup, a similar approximation scheme can be used. This case is much simpler, since the response function does not depend upon the azimuthal angle of incidence of the particles. (Except for a small effect due to the rectangular structure of grids themselves. If the grids are mounted such that the wires of a given grid are not parallel to the wires of the other grids, this effect will be minimized.) The sensitive area can be approximated by a single trapezoid, and the grid transparency term contains one sum of gaussians, rather than the product of two sums of gaussians. The integration over azimuth angle then yields a modified Bessel function, which can be approximated by a sum of exponentials to permit analytic evaluation of the integral over the magnitude of the tangential velocity. The response function of the D-cup of the Voyager PLS instrument is discussed in detail in Reference 15.

## 6. Experimental Test of the Response Function

In order to test our theoretical response function, we have analyzed data taken by Voyager 1 during a cruise maneuver. Voyager is a three-axis stabilized spacecraft, and most of the time it is oriented such that the main sensor symmetry axis, which is parallel to the spacecraft's main antenna, is pointed toward the Earth. Since the angular separation between the Earth and the sun, as viewed from the outer solar system, is small, the solar wind direction was usually almost parallel to the main sensor symmetry axis. In this configuration the "unity response" approximation to the cup response (all incident particles which are not stopped by the modulator voltage reach the

collector, but the aperture area is corrected for the transparency of the grids at normal incidence) is good. During the cruise maneuver, however, the spacecraft performed a series of rotations, some of which involved rotating the main antenna away from the Earth.

The data were taken over a period of 90 minutes on 14 September, 1978, when Voyager 1 was 4.1 AU from the sun. The solar wind bulk speed during the maneuver varied between 368 and 378 km/sec, while the thermal speed varied between 14 and 20 km/sec. Data were taken simultaneously in all four cups. Two such spectra are shown in Figures 14 and 15. The figures consists of  $I_k/(\phi_{k+1}-\phi_k)$  plotted versus  $v_k$  for each cup. The staircases are the data, while the smooth curves are the "best fit" simulations. The fits are excellent, correctly reproducing the location, height, and shape of each peaks in all of the cups in which there is a signal. For the spectra of Figure 14, the angles between the bulk velocity and the cup normals for the A, B, C, and D cups were  $38^\circ$ ,  $72^\circ$ ,  $56^\circ$  and  $124^\circ$ , respectively, while for the spectrum of Fig. 15 the angles were  $67^\circ$ ,  $34^\circ$ ,  $52^\circ$ , and  $56^\circ$ , respectively.

As an illustration of the extent to which we are actually testing our response function using this process, consider Figures 16 and 17. Figure 16 is the same spectrum as Figure 14, except that the smooth curve is a simulation using the parameters derived from the fit of Fig. 14 with the assumption of unity response. Notice that although the peaks are all in the right place due to the effect of the sharply peaked distribution function, the heights and shapes are all wrong. It should be pointed out that the current in the B cup of this spectrum is only about 4% of what the current would be if the same beam were at normal incidence.

An even more striking example is shown in Fig. 17. While the measurements were being taken, the spacecraft was rotating at a rate of one

rotation every 33 minutes. Since the instrument takes 0.24 seconds to measure a single channel, and the same channel is measured simultaneously in all four cups, the peak in the B-cup (channel 46) was measured about 5 seconds later than the peak in the A-cup (channel 24) was measured. During that time, the spacecraft rotated about  $0.9^\circ$ . For the fit shown in Fig. 15, this rotation was compensated for, while for the fit shown in Fig 17 the effect of this small rotation was neglected. Our theoretical response function is sufficiently good that failure to account for this rotation of less than  $1^\circ$  made the fit noticeably worse! The quality of the fits to the data taken during the cruise maneuver has convinced us that our theoretical response function represents the true response function of the Voyager PLS experiment within a few percent for all angles of incidence.

#### 7. Acknowledgements

We would like to thank Herb Bridge, John Belcher, and Alan Lazarus for helpful discussions. This work was supported under JPL Contract 953733 and NASA contract NSG 22-009-015.



## References

- <sup>1</sup>Vasyliunas, V.M., in Methods of Experimental Physics 9B,49, R. A. Lovberg, ed. Academic Press NY 1971
- <sup>2</sup>Bridge, H.S., C. Dilworth, A.J. Lazarus, E.F. Lyon. B.B. Rossi, and F. Sherb, I.G. Bull. 55,12, 1962
- <sup>3</sup>Neugebauer, M. and C.W. Snyder, Science 138,1095, 1962
- <sup>4</sup>Lazarus, A.J., H.S. Bridge, J.M. Davis, and C.W. Snyder, in Space Research VII p 1296 North Holland, Amsterdam 1965
- <sup>5</sup>Bridge, H.S., A.J. Lazarus, C.W. Snyder, E.J. Smith, L. Davis jr., P.J. Coleman jr., and D. E. Jones, Science 158,3809,1665, 1962
- <sup>6</sup>Lazarus, A.J., H.S. Bridge, and J. Davis, J. Geophys. Res. 71,15,3787, 1966
- <sup>7</sup>Lazarus, A.J., G.L. Siscoe, and N.F. Ness J. Geophys. Res. 73,7,2399, 1968
- <sup>8</sup>Lyon, E., A. Egidio, G. Pizzella, H.S. Bridge, J. Binsack, R. Baker, and R. Butler, in Space Research VIII, North Holland, Amsterdam 1968
- <sup>9</sup>Bridge, H.S., J.W. Belcher, R.J. Butler, A.J. Lazarus, A.M. Mavretic, J.D. Sullivan, G.L. Siscoe, and V.M. Vasyliunas, Sp. Sci. Rev. 21,259, 1977
- <sup>10</sup>Gazis, P. R. and A. J. Lazarus, Geophys. Res. Lett. 9,4,431 1982
- <sup>11</sup>Bagenal, F., and J. D. Sullivan, J. Geophys. Res. 86,A10,8447 1981
- <sup>12</sup>McNutt, R. L., J. W. Belcher, and H. S. Bridge, J. Geophys. Res. 86,A10,8314, 1981
- <sup>13</sup>Lazarus, A. J., and R. L. McNutt, J. Geophys. Res. 88,11,8831, 1983
- <sup>14</sup>Barnett, A. S., submitted to J. Geophys. Res.
- <sup>15</sup>Barnett, A.S; NASA technical report CSR-TR-84-1 1984

## Figure Captions

Figure 1 The Voyager plasma science (PLS) experiment, showing the relative orientations of the three cups.

Figure 2 Cross section of a PLS main sensor cup. The grids are numbered 1 through 9, and the directions of  $\hat{y}$  and  $\hat{z}$  axes (cup coordinates) are shown.

Figure 3 PLS main sensor aperture and collector areas. Note direction of axes for cup coordinates:  $\hat{z}$  points into the cup.

Figure 4 Modulator voltage and collector current versus time.  $\phi_k$  is the modulator grid threshold voltage of the k-th channel,  $\Delta\phi_k$  is the voltage width of the k-th channel,  $I_k^*$  is the collector current when the modulator grid voltage is  $\phi_k$ , and  $I_k$  is the current in the k-th channel.

Figure 5 Model potential versus z for a PLS main sensor cup. The numbered tick marks on the z-axis correspond to the locations of the grids (see Figure 2). The tick mark labelled c corresponds to the collector.

Figure 6 Definition of the shift vector. The figure shows the outline of the collector of one of the main sensor cups, with the image of the aperture in the collector superposed on it. An incident monoenergetic beam of particles will have the shape of the aperture as it travels through the cup. The shift vector  $\vec{S}$  is the vector which lies in the collector plane and points from the point directly underneath the center of the long side of the aperture to the corresponding point on the image of the aperture in the incident beam.

Figure 7 The sensitive area of a main sensor cup. The figure shows the 16 distinct regions in which there is a different functional dependence of the sensitive area on the shift vector.

Figure 8 Main sensor sensitive area versus  $S_y/h$ .

Figure 9 Geometry for grid transparency calculation. A beam of particles incident on a grid of parallel, cylindrical wires is shown.  $\alpha$  is the angle between the beam direction and the normal to the plane of the grid,  $L$  is the distance between the centers of two adjacent wires, and  $d$  is the wire diameter. The wires run in the  $\hat{y}$ -direction, and the  $\hat{z}$ -direction is normal to the grid plane, with  $+\hat{z}$  making an acute angle with the direction of the incident beam.

Figure 10 Main sensor sensitive area versus  $S_y/h$  (trapezoidal approximation). Compare with Figure 8.

Figure 11  $Y_u$  and  $Y'_u$  versus  $S_x/h$ .

Figure 12 3-D plot of the sensitive area versus  $S_x$  and  $S_y$  in the trapezoidal approximation.

Figure 13 3-D plot of the full response function, computed using the trapezoidal approximation for the sensitive area and the "exact" expression for the grid transparency.

Figure 14 Reduced distribution function versus velocity for cruise maneuver spectrum 1. The staircases are the data, while the smooth curve is the fit.

Figure 15 Reduced distribution function versus velocity for cruise maneuver spectrum 2. The staircases are the data, while the smooth curve is the fit.

Figure 16 Reduced distribution function versus velocity for cruise maneuver spectrum 1. The staircases are the data, while the smooth curve is a simulation done assuming "unity" response using the plasma parameters determined from the fit which is plotted in Figure 14. Note that the locations of the peaks in the simulation are correct, but their heights and shapes are wrong.

Figure 17 Reduced distribution function versus velocity for cruise maneuver spectrum 2. The staircases are the data, while the smooth curve is the fit. The change in the orientation of the spacecraft between the time of the peaks in the different cups was not compensated for. Compare to Figure 15.

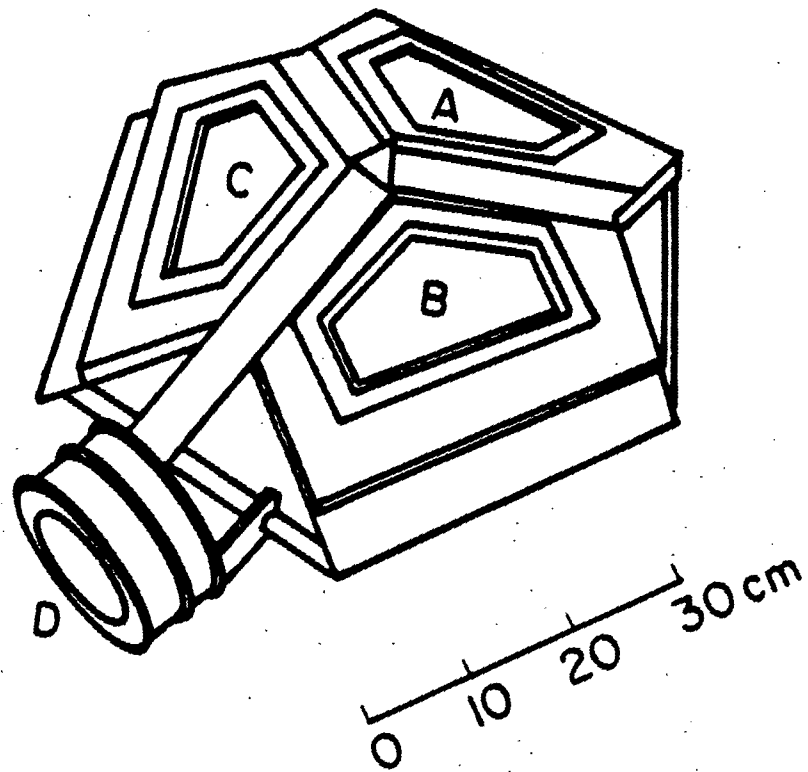
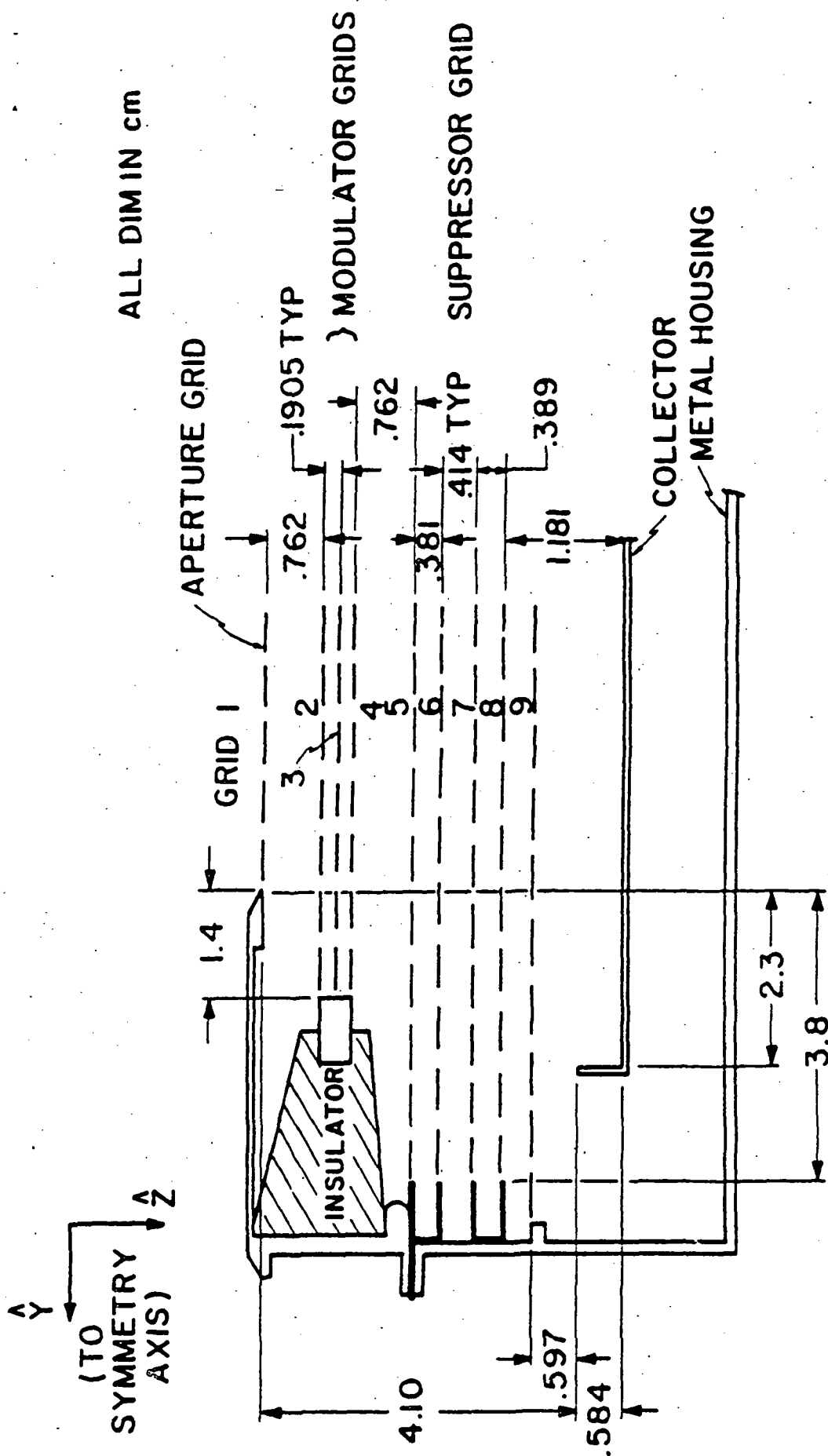
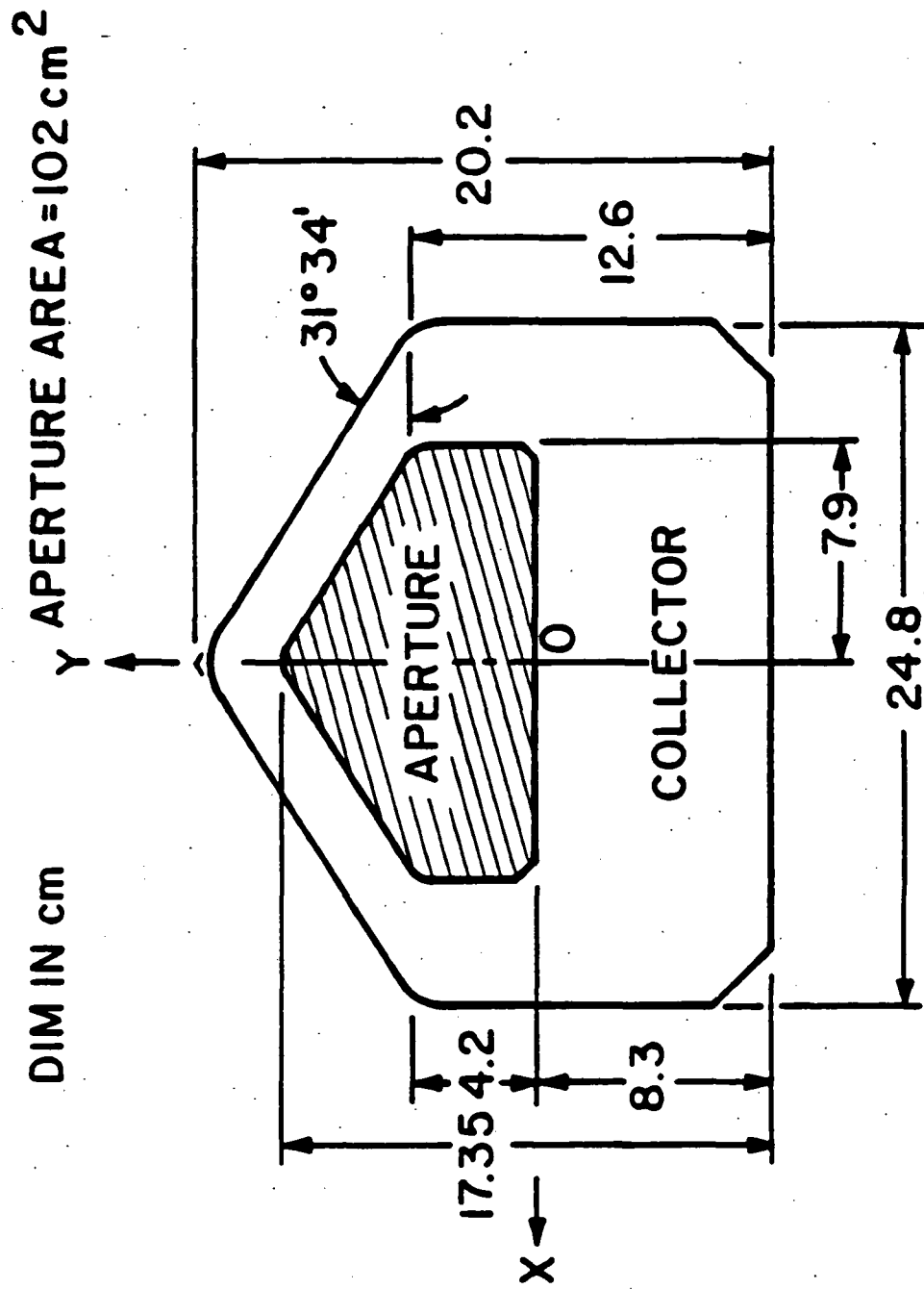


Figure 1



MAIN SENSOR  
VERTICAL CUT OF UPPER SEGMENT

Figure 2



MAIN SENSOR (APERTURE AND COLLECTOR AREAS)

Figure 3

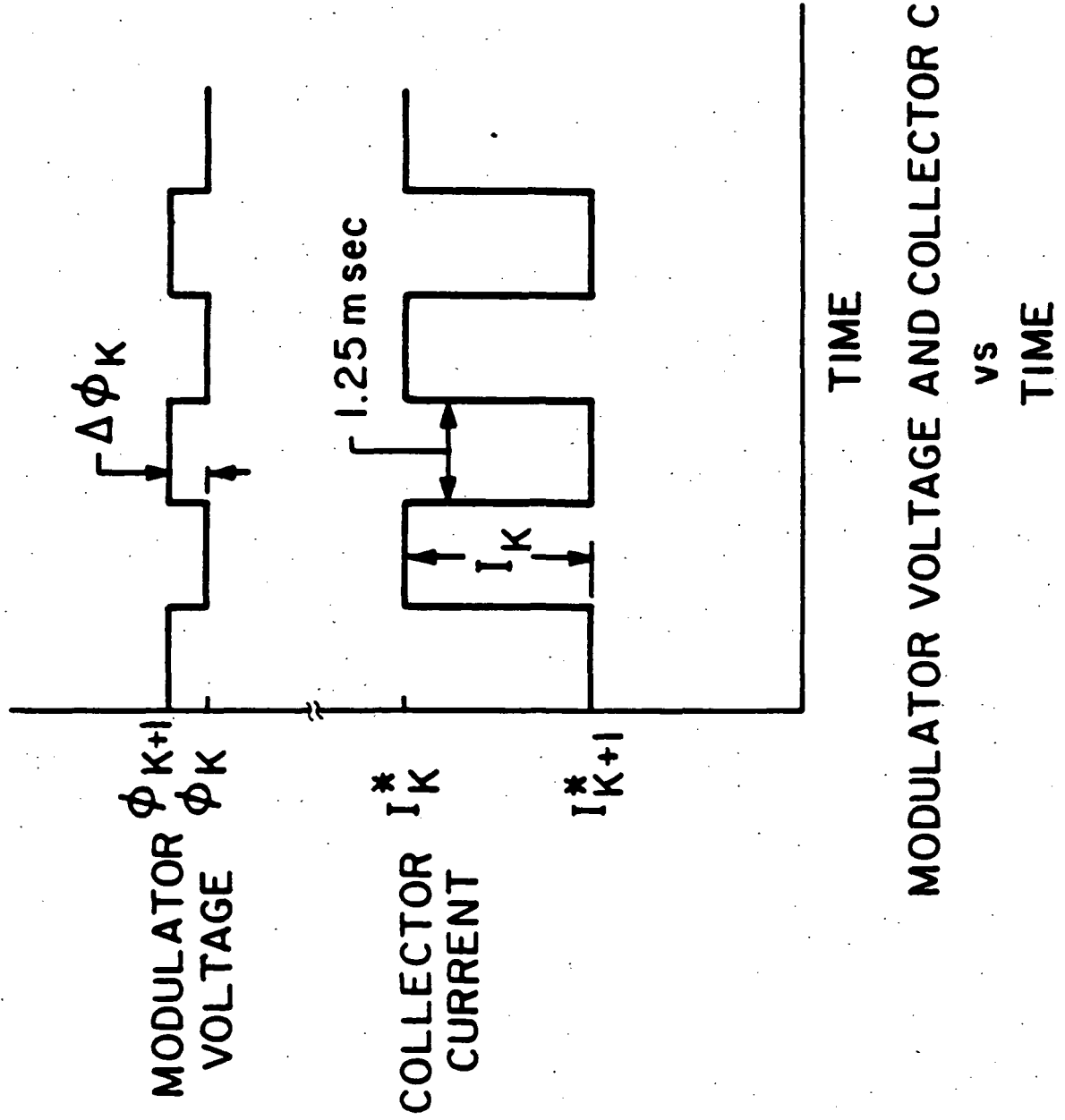


Figure 4



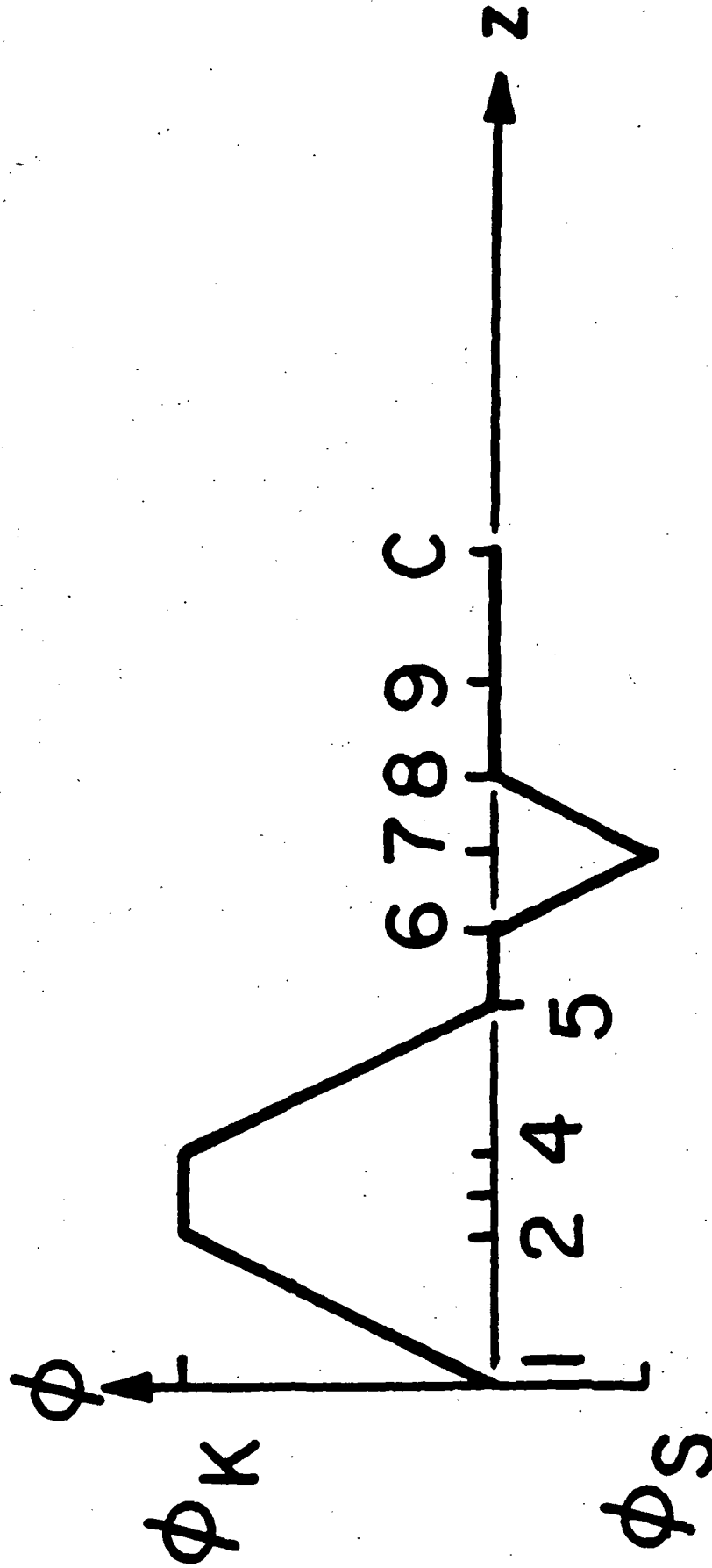
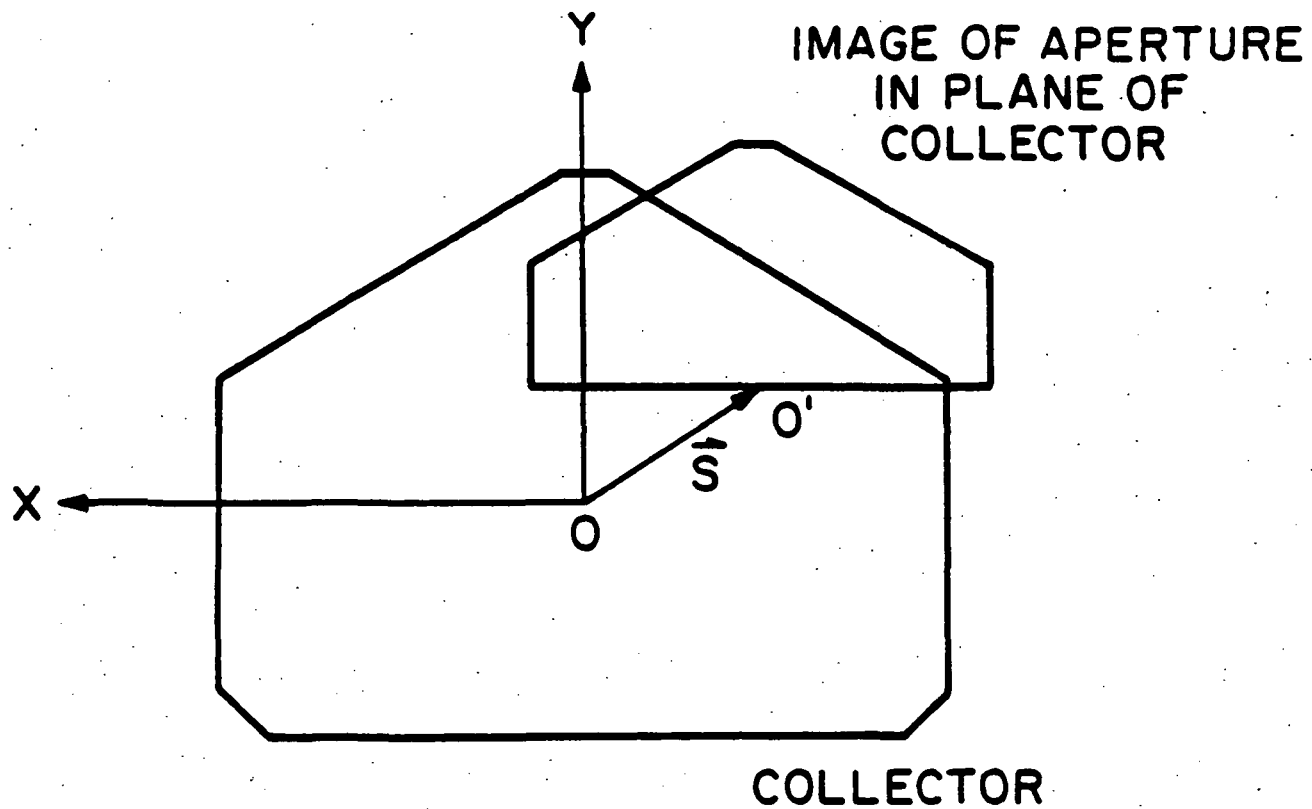


Figure 5



### DEFINITION OF SHIFT VECTOR

Figure 6

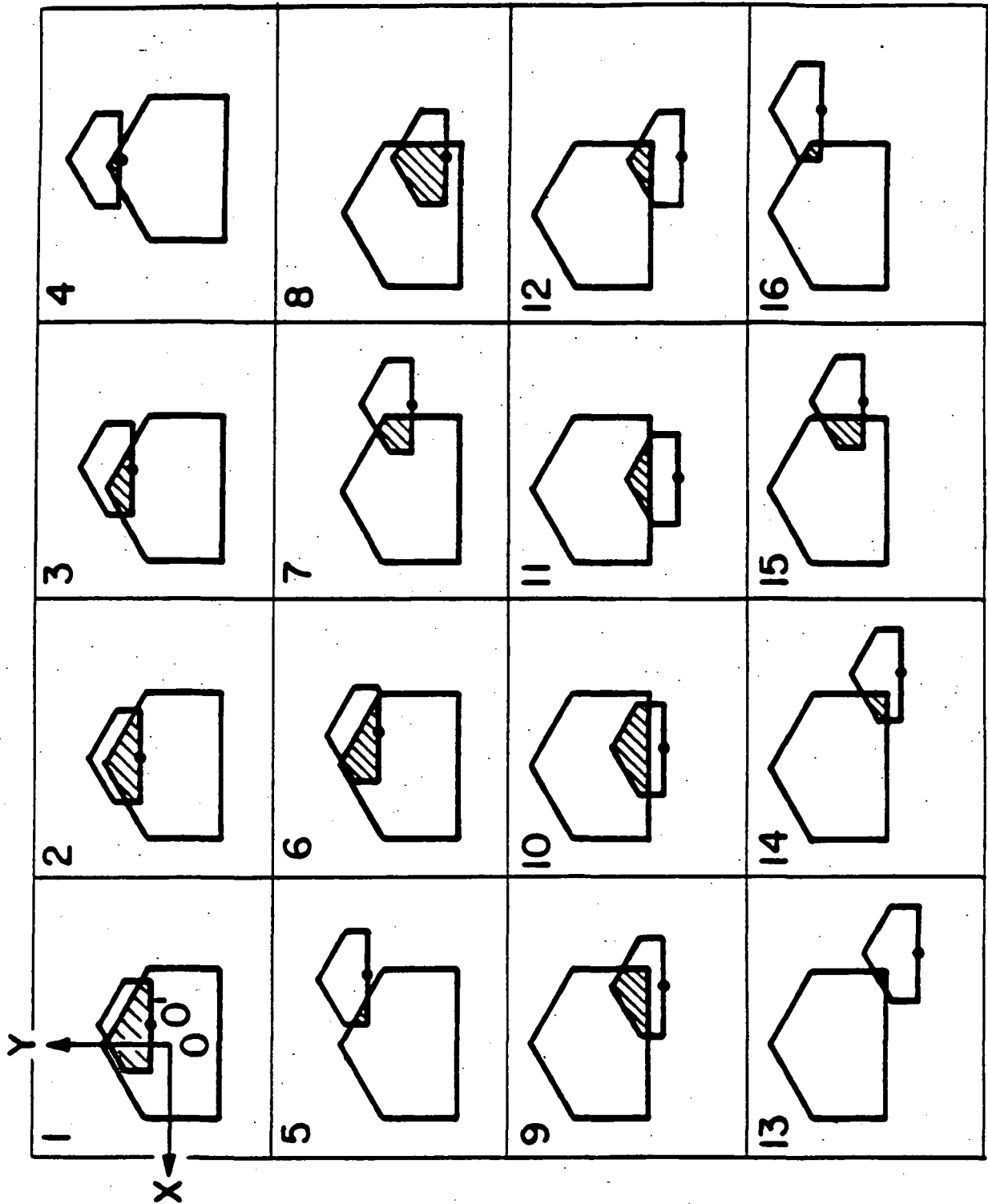
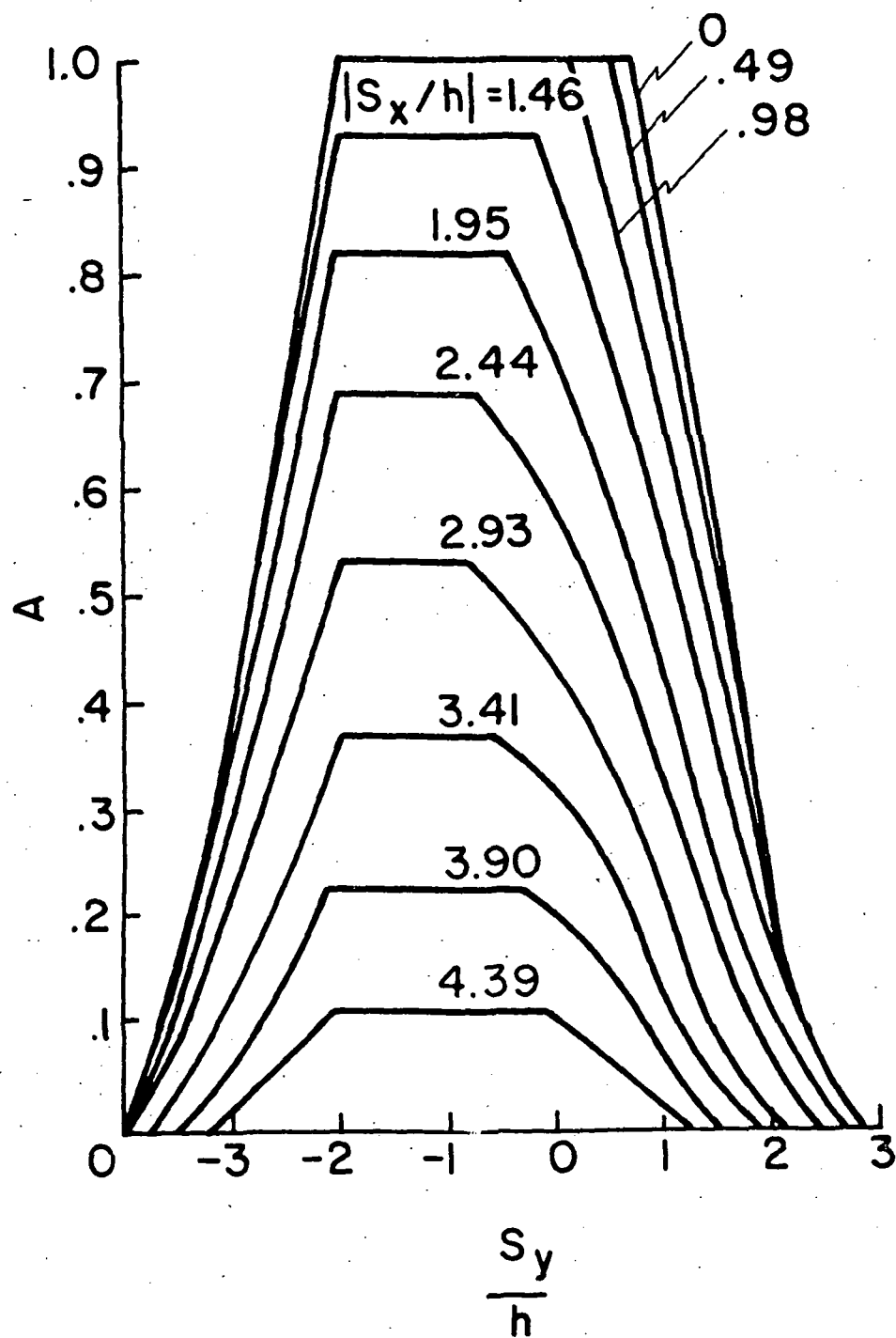
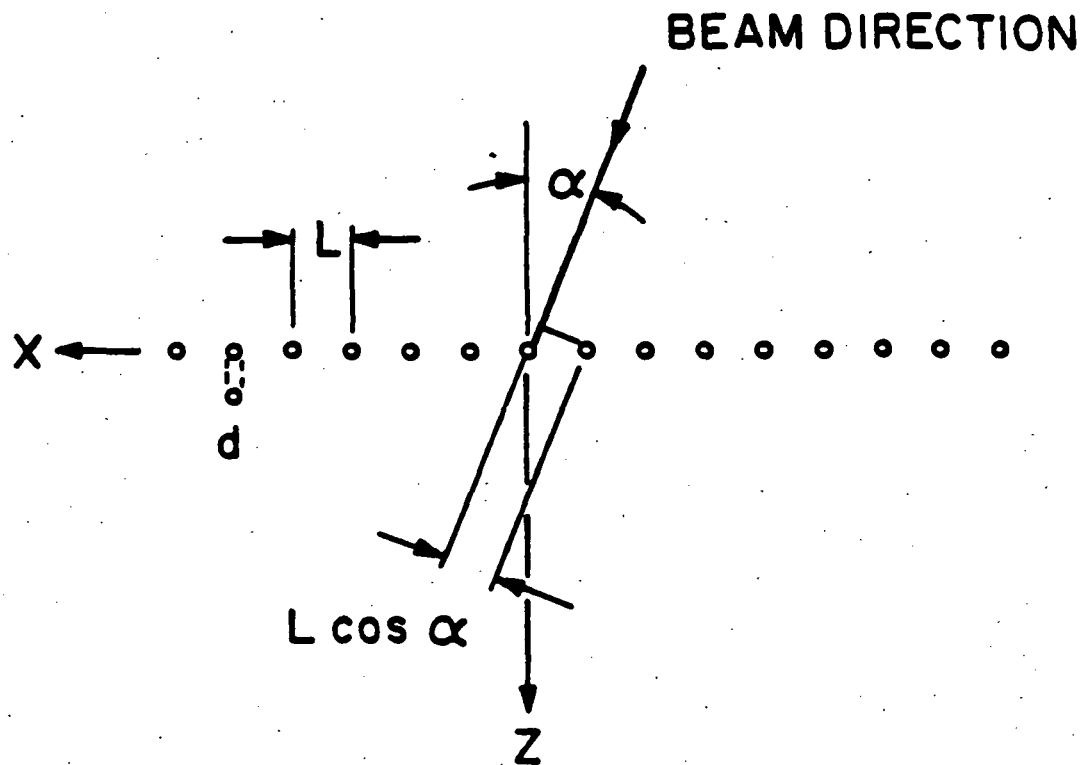


Figure 7

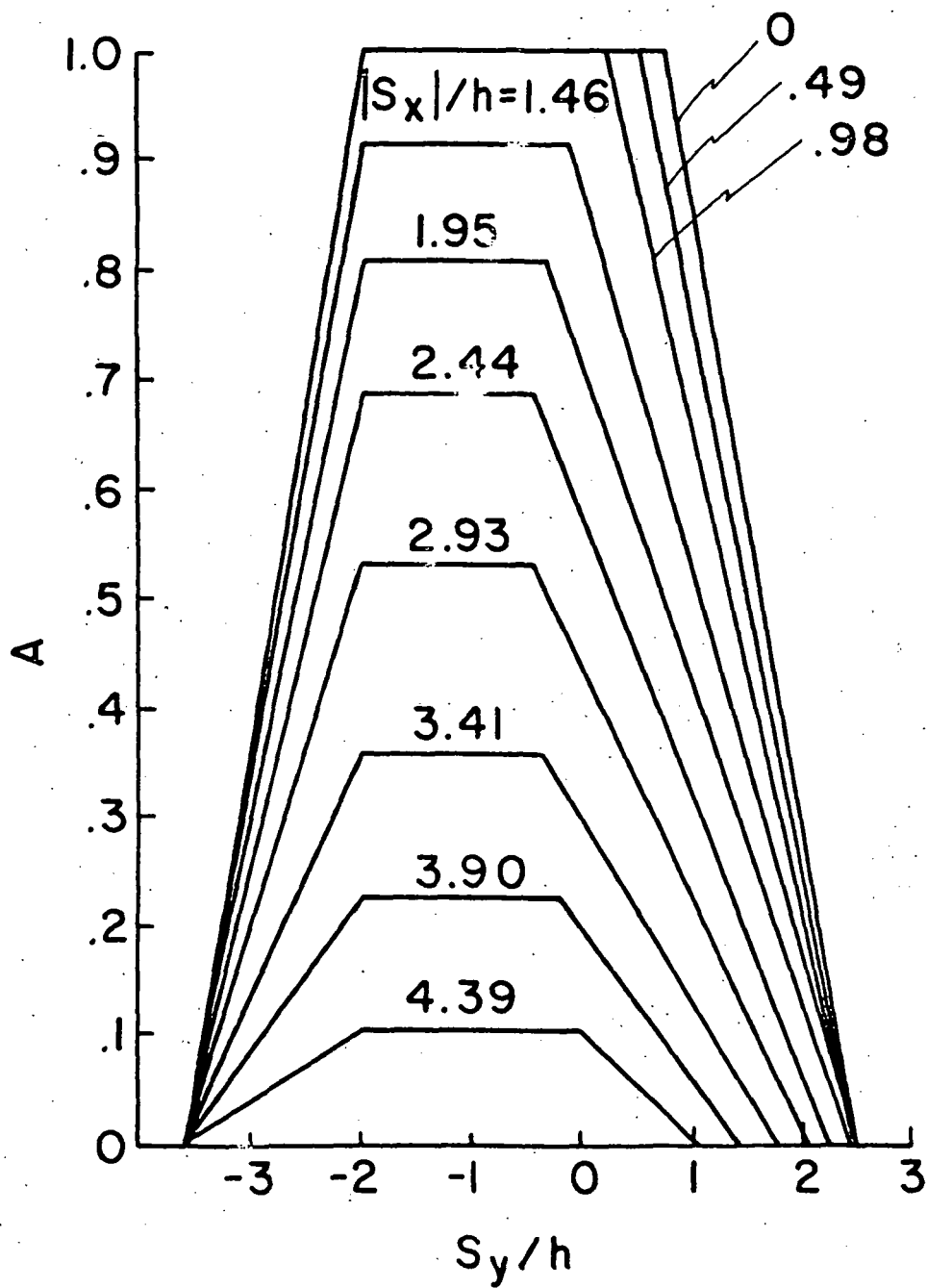


MAIN SENSOR SENSITIVE AREA vs  $S_y/h$



## GEOMETRY FOR GRID TRANSPARENCY

Figure 9



MAIN SENSOR SENSITIVE AREA vs  $S_y/h$   
(TRAPEZOIDAL APPROXIMATION)

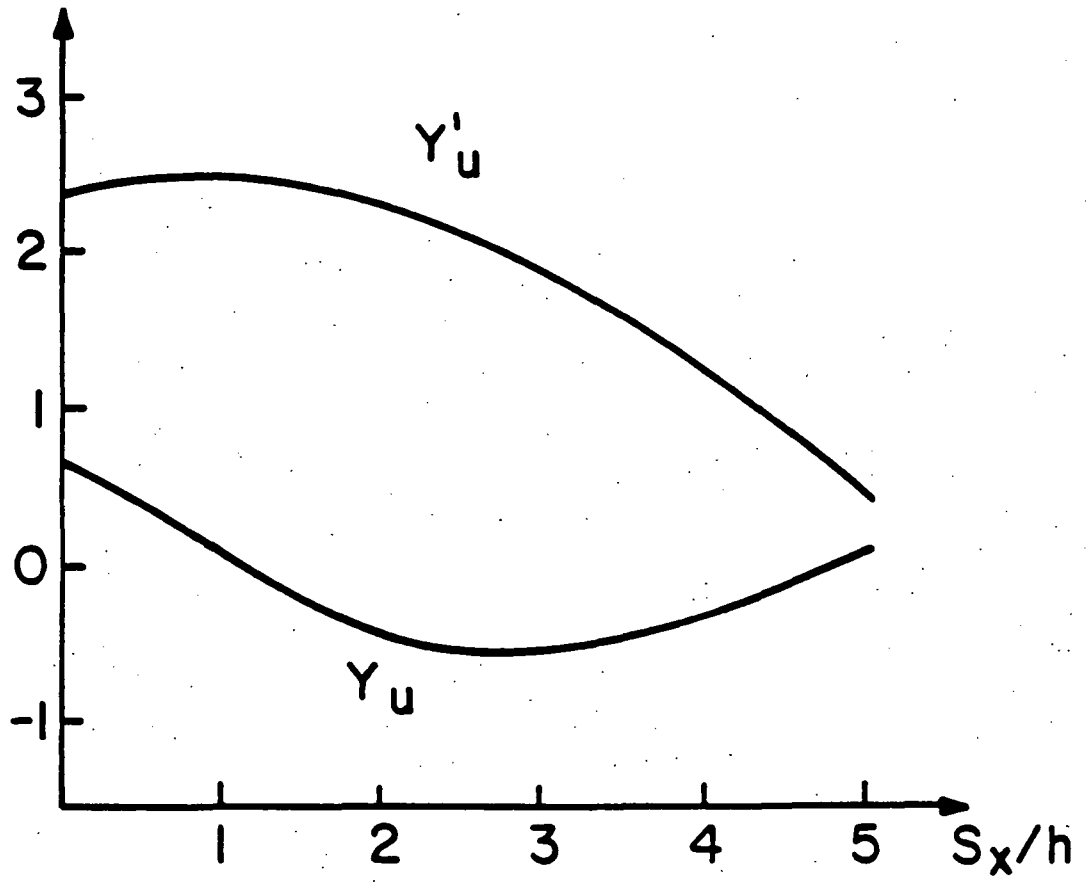


Figure 11

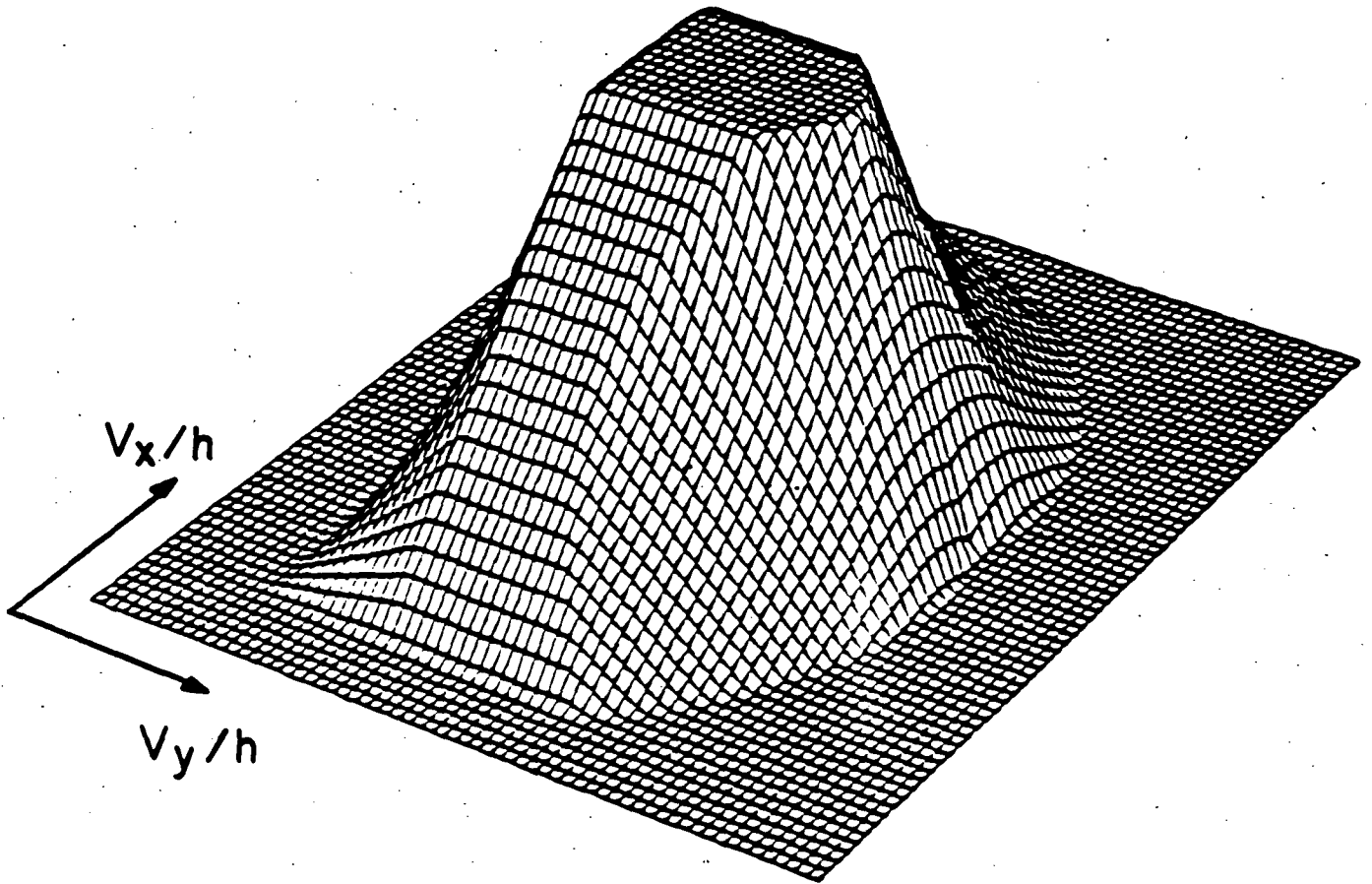


Figure 12



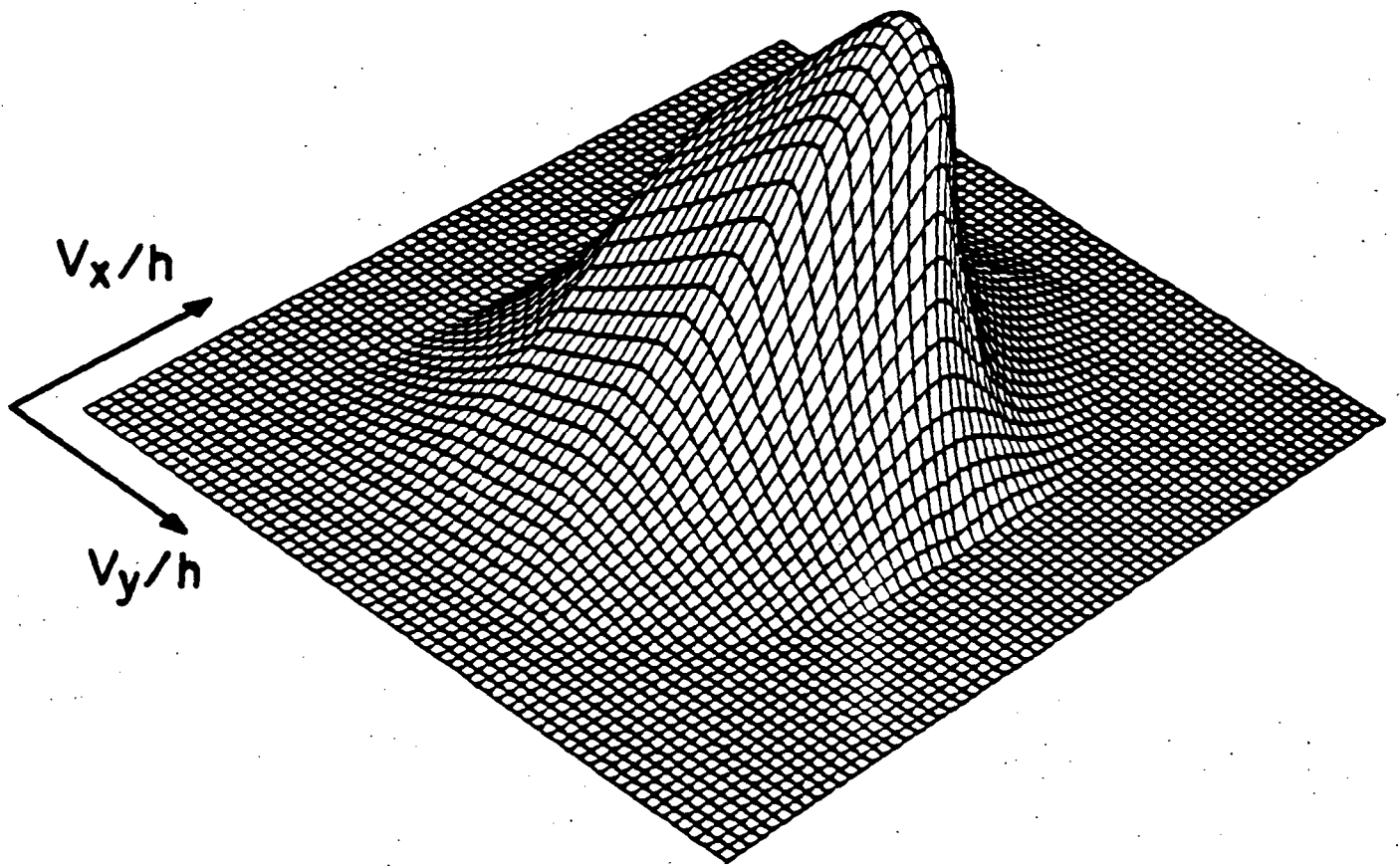
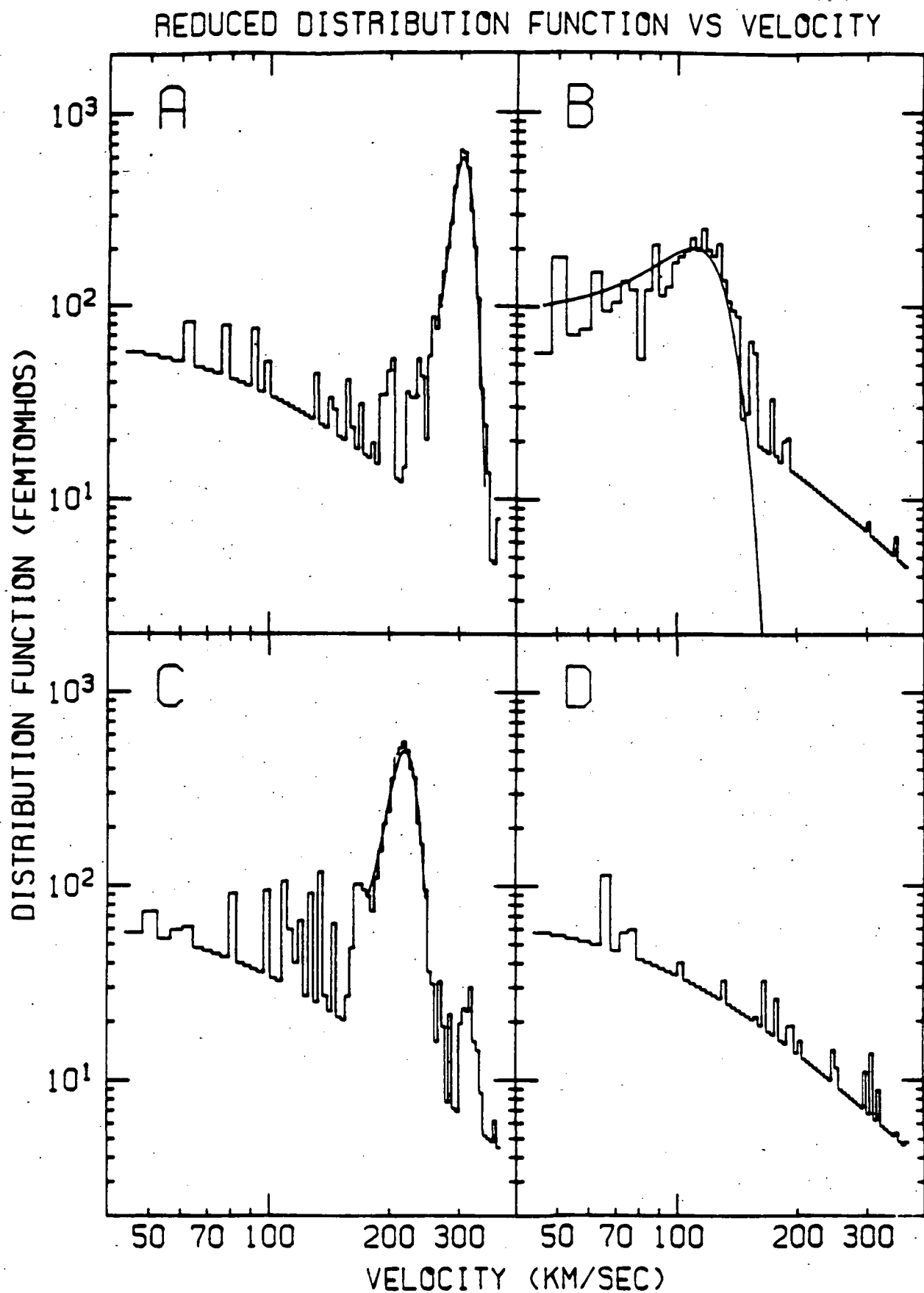


Figure 13



Preceding Page Blank

Figure 14

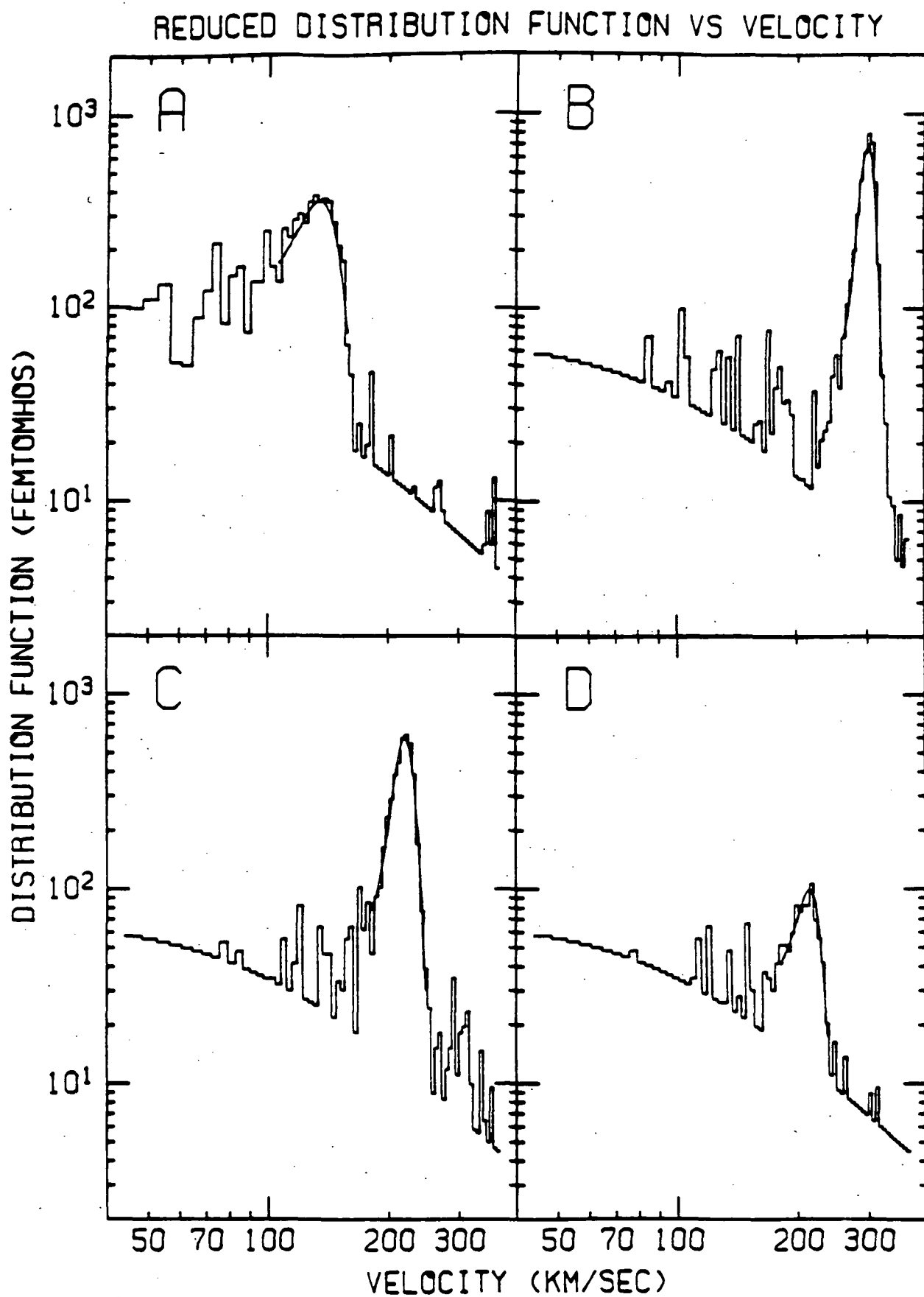


Figure 15

# REDUCED DISTRIBUTION FUNCTION VS VELOCITY

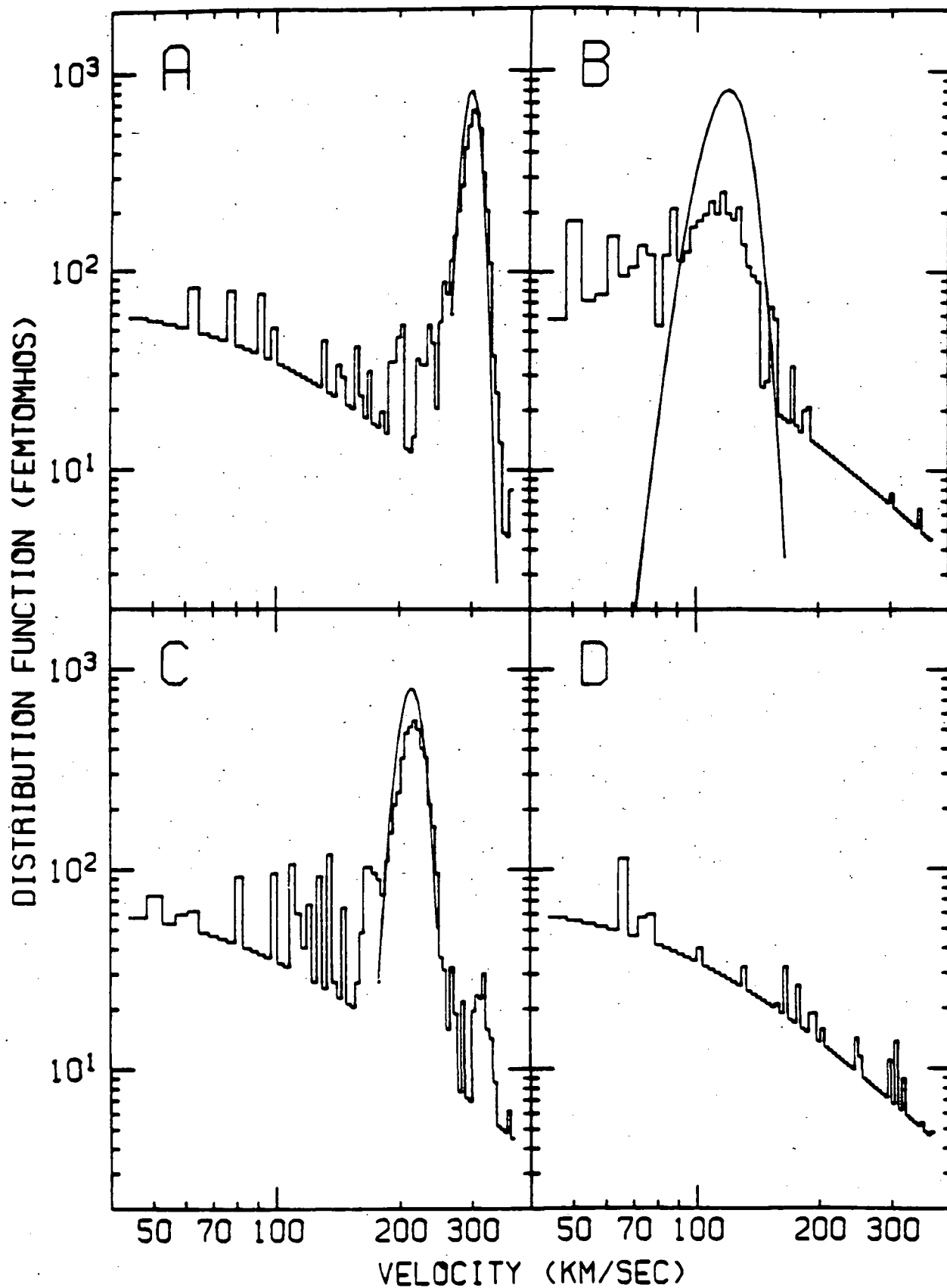


Figure 16

# REDUCED DISTRIBUTION FUNCTION VS VELOCITY

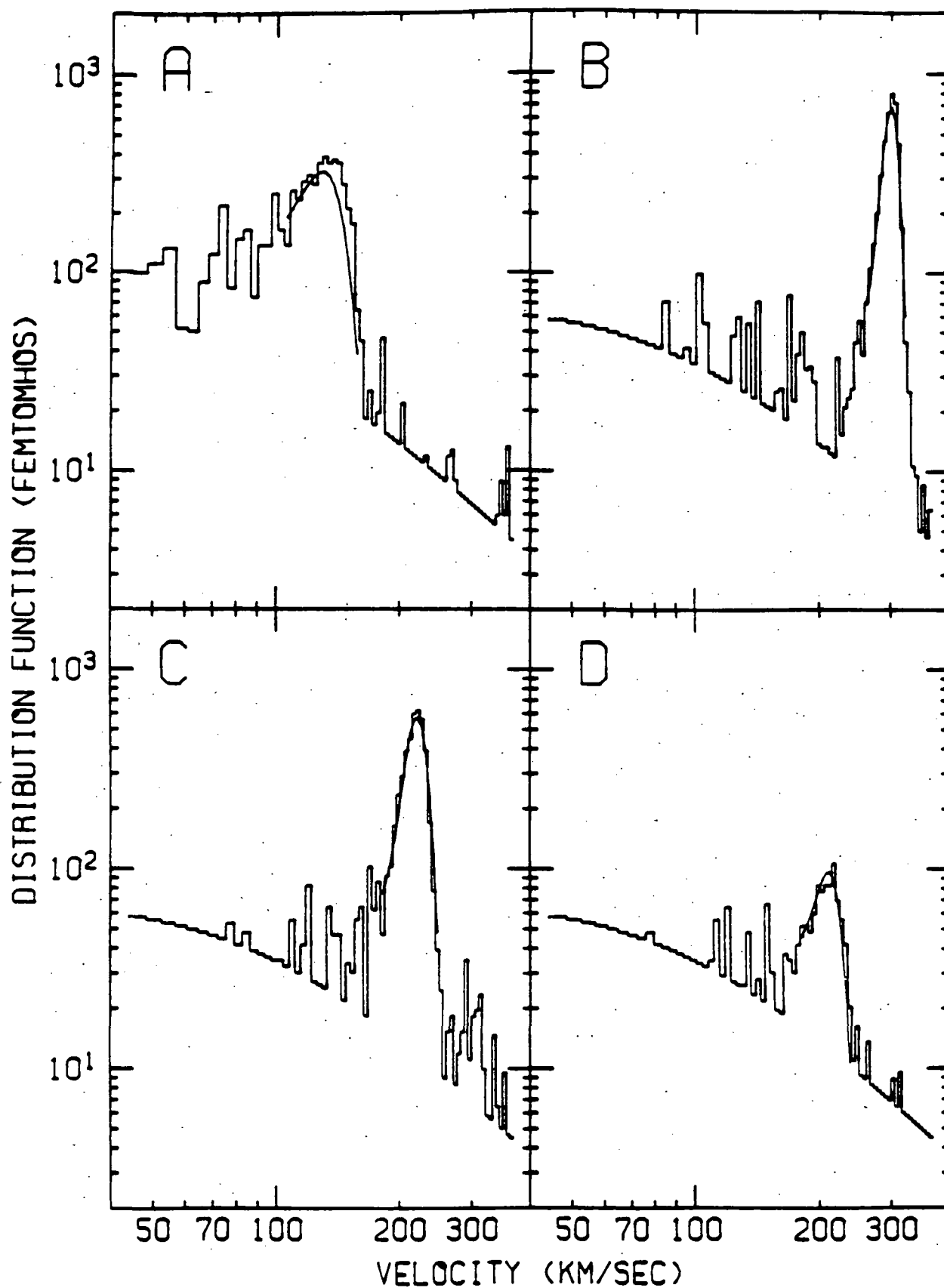


Figure 17